Rayleigh Fading Compensation for 16QAM Using FFT

Eiji Okamoto, Huan-Bang Li, and Tetsushi Ikegami, *Member, IEEE*

Abstract— **Pilot symbol assisted modulation (PSAM) has been proposed to overcome the Rayleigh fading. However, as the fading rate becomes more rapid, it is difficult to provide an exact interpolation with conventional PSAM.**

To compensate for the fast Rayleigh fading, a PSAM which calculates in the frequency domain rather than the time domain as in conventional PSAM is proposed. Although this PSAM scheme only needs the zero interpolation for fading estimation, it provides a very accurate estimate even in relatively fast Rayleigh fading environments.

We introduce this PSAM using fast Fourier transform (FFT) and apply it to 16QAM, and then show some results of computer simulations.

Keywords— **Fading Compensation, Pilot Symbol, 16QAM, FFT.**

I. Introduction

FADING is one of the main problems in land mobile communications (LMC) because it introduces irreducible error floors and seriously degrades the quality of communication links. This fading must be compensated for high-quality communications.

Transmissions at a higher rate and higher capacity are becoming increasingly required especially in digital communications. However, expanding the bandwidth is difficult because of the limited spectrum for LMC. Quadrature amplitude modulation (QAM) is one effective modulation technique used in achieving high bit rate transmission without increasing the bandwidth, and is therefore a competitive candidate for LMC. However, QAM requires more exact fading compensation because QAM signals have both the amplitude and phase information, and they must both be compensated accurately. Thus, accurate fading compensation techniques for digital communications with QAM are very important.

Pilot symbol assisted modulation (PSAM) is a well-known fading compensation technique for LMC and has been studied by many authors. This technique employs inserted pilot symbols. In the transmitter, a known pilot symbol, which is usually assigned as one of the outermost points of the modulated signal constellation, is inserted periodically in the transmitted symbol sequence. Then the receiver extracts the fading of the channel at pilot symbols. From the fading at pilot symbols, we estimate the fading at the data stream and remove it. Some estimate techniques have been proposed [1], [2], [3], and they have been applied to various systems and modulations which have fading channels [4], [5]. Furthermore, there are some studies on PSAM treating the fading, which is not flat Rayleigh fading [6]. These techniques use various functions such as Gaussian, Bessel, etc. in the time domain to estimate fading, and then compensate it. Recently, as the frequency used in LMC has become higher and higher, the fading rate has become more and more rapid, and robust fading compensation is needed. However, with these conventional methods, the estimate may be derived less accurately or the estimate functions and the coefficient of functions tend to become much more complex.

It should be noted that the Rayleigh fading is a kind of band-limited process. Concentrating on this characteristic, we propose a method of using fast Fourier transform (FFT) [7] to execute the channel estimation with the PSAM. In this method, received pilot symbols are translated once into the frequency domain. After that the zero symbols are inserted into them, and the result produced is reconverted into the time domain. The calculated result becomes the estimated fading. Since this method needs only zero insertion in the fading estimation, it is simple; however, it produces very accurate estimation. The main difference between this method and the conventional methods of PSAM is that the fading estimation proceeds in the frequency domain rather than the time domain.

In this paper we introduce this method. First, a detailed description of the system construction and the strategy of the method are presented. Then we investigate the theoretical degradation in an additive white Gaussian noise (AWGN) environment. The degradation of digital transmissions in the Rayleigh channel has been studied [8], [9]. We investigate the degradation in the Rayleigh fading environment for the proposed method with QAM. It is confirmed that the degradation with the proposed method in a relatively fast Rayleigh fading environment is almost the same as that in an AWGN environment; that is, the proposed method can successfully follow the fast fading.

Examples of applying this method to 16QAM are given through computer simulations. The effects of some parameters are also investigated.

II. Fading Compensation Method Using FFT

A. Frame Format of PSAM

The Fading processes like Rayleigh or Rician are one of the band-limited processes, and the bandwidth is f_D Hz when the maximum Doppler frequency is f_D.

Fig. 1 shows the frame format studied in this paper. We take N symbols as a frame, and insert a known pilot symbol at the beginning of each frame, and thus the data stream in

E. Okamoto and H.-B. Li are with the Communications Research Laboratory, at the Ministry of Posts and Telecommunications, 893-1 Hirai, Kashima, Ibaraki 314, Japan (e-mail: oka@crl.go.jp).

T. Ikegami is with the Department of Electronics and Communications, Meiji University, Japan.

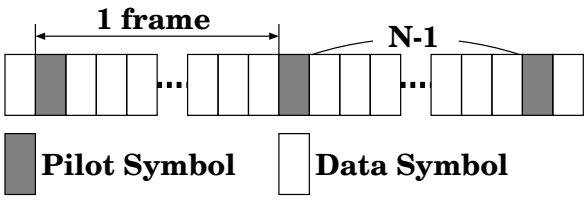

Fig. 1. Frame format.

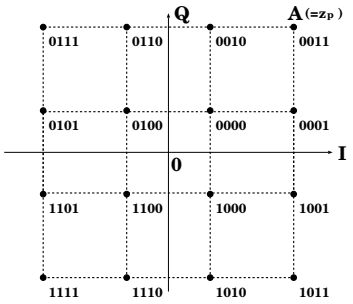

Fig. 2. Gray-coded 16QAM.

one frame includes $N-1$ symbols. The fading information on pilot symbols in the channel can be obtained. Using this fading information, fading on the whole symbol stream can be calculated under the following condition according to the sampling theorem:

$$f_D T_s \leq \frac{1}{2N} \tag{1}$$

where T_s is a symbol interval.

Fig. 2 shows the signal constellation of Gray-coded 16QAM, and the point A is adopted as the pilot symbol z_p at the beginning of a frame. Although the pilot symbols can be selected from any point in Fig. 2, from the view point of the signal power, we take point A which is one of the four outermost points, and is effective to decrease the noise influence.

B. System Model

The baseband system block diagram is shown in Fig. 3. TX data bits are mapped every four bits into one of the sixteen signal points of 16QAM of Fig. 2. Then, known pilot symbols are periodically inserted, and the composite signal is band-limited by the low-pass filter (LPF). After that, it is transmitted over a Rayleigh fading channel with the AWGN. At the receiver, the received signal is first band-limited by the LPF. The fading of the received signal is compensated using an estimate obtained from the received pilot symbols. Finally, the received data is decided.

The received signal has a complex envelope, which is given by

$$r(t) = c(t)s(t) + n(t) \tag{2}$$

where $c(t)$ is the complex channel gain including fading and frequency offset, and $n(t)$ is the equivalent low-pass AWGN

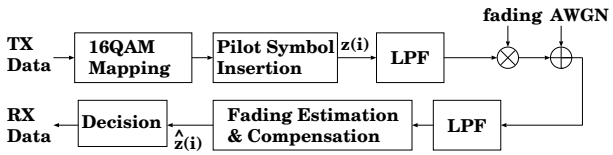

Fig. 3. System block diagram.

with a variance of σ^2; $s(t)$ is given by

$$s(t) = \sum_{i=-\infty}^{\infty} z(i)p(t - iT_s) \tag{3}$$

where $z(i)$ is the ith symbol value of 16QAM including the pilot symbol, and $p(t)$ is the raised cosine pulse given by

$$p(t) = \frac{\sin(\pi t/T_s)}{\pi t/T_s} \cdot \frac{\cos(\pi \alpha t/T_s)}{1 - (2\alpha t/T_s)^2} \tag{4}$$

where α is the roll-off factor. We used an equal root allocation for the filter at the transmitter and receiver with the roll-off factor of $\alpha = 0.5$. To simplify the study we assume in the following that the clock and frame synchronization is completely obtained. Then, after LPF and sampling we get the discrete signal:

$$r(i) = c(i)s(i) + n(i) \tag{5}$$

where $s(i) = z(i)$ in perfect synchronization.

Denoting the channel estimate by $\hat{c}(i)$ and the fading-compensated data by $\hat{z}(i)$, we have

$$\hat{z}(i) = \frac{c(i)z(i) + n(i)}{\hat{c}(i)}. \tag{6}$$

After the decision on $\hat{z}(i)$, we get the RX data bits.

C. Fading Estimation Using FFT

Fig. 4 and 5 show the principle of the proposed method. Fig. 4 (a) illustrates the periodic fading process cut by a rectangular window and sampled every T_p sec, and its spectrum. The fading process in Fig. 4 (a) is repeated with a period of T_{FL}, because this series is used for the discrete Fourier transform which needs a periodical process. In this fading process, if the Nyquist condition, $f_D T_p \leq 1/2$ is satisfied, the spectrum includes all components of fading in the T_{FL} section. Theoretically, there are zero points between the repetitious non-zero spectra in Fig. 4 (b). To carry out the interpolation, we inserted zero symbols between these two non-zero spectra. Fig. 5 (b) shows the results of doing this. By transforming this series into the time domain, an interpolated time series is obtained as Fig. 5 (a) shows. Zero interpolation in the frequency domain thus plays the same role as symbol interpolation in the time domain. We used this principle since it is simple.

The fading estimate operation using FFT is shown in Fig. 6, and the frame structure used in the calculation in Fig. 6 is shown in Fig. 7. We calculate and estimate a fading series of N_p frames at a time from $2N_p$ pilot symbols.

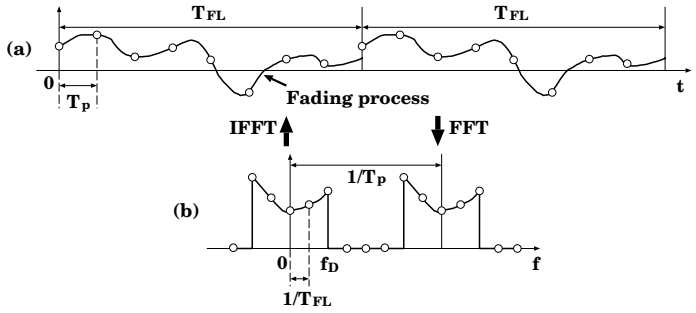

Fig. 4. The periodic fading process and its spectrum.

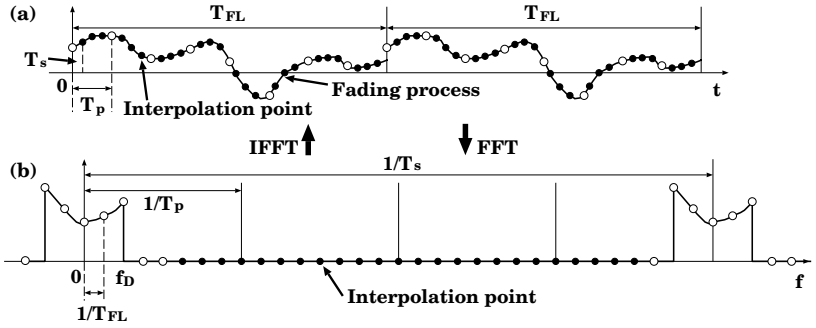

Fig. 5. Zero inserted spectrum and interpolated fading series corresponding to the spectrum.

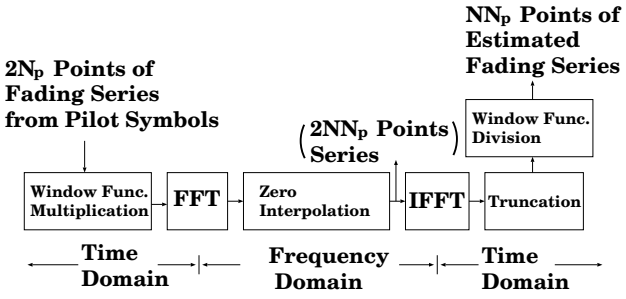

Fig. 6. Configuration of fading estimate operation.

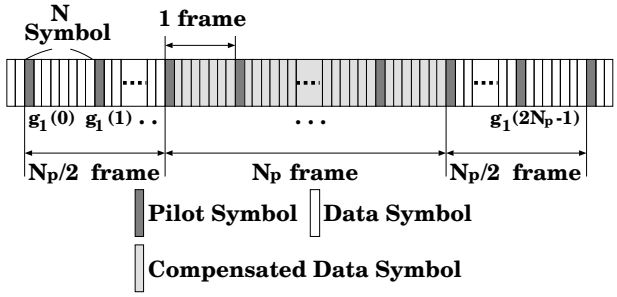

Fig. 7. Frame structure in calculation.

First, the $2N_p$ symbol fading series $g(l)(l = 0, 1, \cdots, 2N_p - 1)$ is obtained by dividing the received pilot symbols by z_p:

$$g(l) = \frac{r(l)}{z_p}. \tag{7}$$

Since FFT and the inverse fast Fourier transform (IFFT) are used in calculation, inserting a window function is effective in concentrating the signal spectrum. By inserting it, we can decrease the spectrum power out of the calculating band, and thus reduce the alias effect. This operation increases the precision of estimation.

There are many window functions. We apply a few of them as listed below and compare them:

(a) Hanning window function

$$w_l^{(H)} = \frac{1}{2}\left[1 - \cos\left(\frac{\pi l}{N_p}\right)\right] \tag{8}$$

(b) Parzen window function

$$w_l^{(P)} = 1 - \left|\frac{2l - N_p + 1}{N_p + 1}\right| \tag{9}$$

(c) Welch window function

$$w_l^{(W)} = 1 - \left(\frac{2l - N_p + 1}{N_p + 1}\right)^2 \tag{10}$$

Thus, we get the series:

$$g_1(l) = g(l)w_l, (l = 0, 1, \cdots, 2N_p - 1) \tag{11}$$

and then transform $g_1(l)$ into the frequency domain by using FFT:

$$G_1(n) = \sum_{l=0}^{2N_p-1} g_1(l)\exp(-\frac{j\pi nl}{N_p}). \quad (n = 0, 1, \cdots, 2N_p - 1) \tag{12}$$

Note that although this formula is only a discrete Fourier transform (DFT), we apply FFT in calculation to save time.

Within the range of Eq. (1), this $G_1(n)$ includes all the frequency components of the received fading symbols, and near $n = N_p$, $G_1(n)$ approximately equals zero, while it does take the value of zero theoretically. Then we can interpolate from $2N_p$ symbols to $2NN_p$ symbols with zero interpolation as below:

$$G_1'(m) = \begin{cases} NG_1(m); & [0 \le m \le N_p - 1] \\ 0; & [N_p \le m \le N_p(2N-1) - 1] \\ NG_1(m - 2N_p\{N-1\}); & \\ & [N_p(2N-1) \le m \le 2N_pN - 1] \end{cases} \quad (13)$$

As mentioned above, this zero interpolation in the frequency domain is identical to the interpolation between pilot symbols in the time domain. Since only zero insertion is needed, this interpolation scheme is simple.

Then the time domain series is obtained by transforming $G_1'(m)$ using IFFT:

$$g_1'(k) = \frac{1}{2NN_p} \sum_{m=0}^{2NN_p-1} G_1'(m) \exp(\frac{j\pi mk}{NN_p}) \quad (14)$$
$$(k = 0, 1, \cdots, 2NN_p - 1)$$

For the same reason to save time in Eq. (12), we use IFFT in calculation of Eq. (14) though it is only a formula of the inverse discrete Fourier transform (IDFT).

We truncate the calculated series of $g_1'(k)$ to avoid the alias effect. Usually the alias effect appears more severely at the two ends of the calculating span. Then we pick up only the central half of the NN_p symbols ($NN_p/2 \le k \le 3NN_p/2 - 1$) of the calculated $g_1'(k)$ to maintain high accuracy.

There is also another reason for truncating the series $g_1'(k)$. Recall that before applying FFT, we used a window function to restrict the spectrum. Because of this, we must divide out its components after IFFT. However, the division can not be done because the window functions usually have zero value at the end points, and so it is convenient to exclude the end points through the truncation.

Finally, we get the estimated fading series by removing the components of the window function as follows:

$$\hat{c}(k) = \frac{g_1'(k + NN_p/2)}{w'_{k+NN_p/2}} \quad (15)$$
$$(k = 0, 1, \cdots, NN_p - 1)$$

where w_k' is the same window functions as those of Eqs. (8)–(10) but with a different number of points. This is because that after interpolation, the number of points increased.

(a') Hanning window function

$$w_k^{(H)'} = \frac{1}{2}\left[1 - \cos\left(\frac{\pi k}{NN_p}\right)\right] \quad (16)$$

(b') Parzen window function

$$w_k^{(P)'} = 1 - \left|\frac{2k - NN_p + 1}{NN_p + 1}\right| \quad (17)$$

(c') Welch window function

$$w_k^{(W)'} = 1 - \left(\frac{2k - NN_p + 1}{NN_p + 1}\right)^2. \quad (18)$$

In Eqs. (16)–(18), k takes values from $NN_p/2$ to $3NN_p/2 - 1$.

Since FFT and IFFT are used in calculation, we let N and N_p take the value of the power of 2.

III. BER Performance in AWGN Channel

Next we consider the theoretical BER performance of the proposed scheme in the AWGN channel. The theoretical BER performance of coherently-detected Gray-coded 16QAM in the AWGN environment is [10]

$$P_{bnon}(\gamma_0) = \frac{3}{8}\mathrm{erfc}\left(\sqrt{0.4\gamma_0}\right) - \frac{9}{64}\mathrm{erfc}^2\left(\sqrt{0.4\gamma_0}\right) \quad (19)$$

where $\gamma_0 = E_b/N_0$, E_b is energy per information bit, and N_0 is the one-side noise spectral density.

The performance of PSAM is degraded because of a power loss due to the insertion of pilot symbols. In the proposed scheme, this degradation is given by

$$D_1 = 10\log\left(\frac{N}{N-1}\right) \quad \text{dB}. \quad (20)$$

In addition, there is a degradation D_2 caused by the fading estimation error. This occurs because the received pilot symbols include noise components, and because of the error of the interpolation.

First we compare the received signal power before and after interpolation. Following Eq. (6), the received fading-compensated pilot symbol is represented by

$$g(l) = c(l) + \frac{n(l)}{z_p} \quad (21)$$

where $n(l)$ is the zero mean complex Gaussian noise with a variance of σ^2. The average noise power of $g(l)$ is $\sigma^2/|z_p|^2$.

In Eqs. (8)–(10) and (16)–(18) we applied the window functions to the received symbols. However, we can ignore its effect because these operations affect neither the total power of $g(l)$ nor the noise variance σ^2 on the whole. We can also ignore the operation of truncation since it does not change the SNR of $g(l)$.

From Parseval's theorem, we get the equations below:

$$\sum_{l=0}^{2N_p-1} |g_1(l)|^2 = \frac{1}{2N_p} \sum_{n=0}^{2N_p-1} |G_1(n)|^2 \quad (22)$$

$$\sum_{k=0}^{2NN_p-1} |g_1'(k)|^2 = \frac{1}{2NN_p} \sum_{m=0}^{2NN_p-1} |G_1'(m)|^2. \quad (23)$$

From Eq. (13) we get an equation for the power spectrum as follows:

$$\sum_{m=0}^{2NN_p-1} |G_1'(m)|^2 = N \sum_{n=0}^{2N_p-1} |G_1(n)|^2 N. \qquad (24)$$

Then, from Eqs. (22)–(24) we get

$$\sum_{k=0}^{2NN_p-1} |g_1'(k)|^2 = \sum_{l=0}^{2N_p-1} |g_1(l)|^2 N \qquad (25)$$

which shows that the total power of the received fading signal does not change before and after interpolation.

Next, we assume the estimated fading series $\hat{c}(k)$ as

$$\hat{c}(k) = c'(k) + n_1'(k) \qquad (26)$$

where $c'(k)$ has the estimating error components caused not by the AWGN of the received pilot symbols but by the inaccuracy of the interpolation, and where $n_1'(k)$ is the noise component whose power is $\sigma_1^{'2}$ caused by the AWGN of the received pilot symbols. Then the following equation is obtained from Eq. (6):

$$\hat{z}(k) = \frac{c(k)z(k) + n(k)}{c'(k) + n_1'(k)} \qquad (27)$$

where $c'(k) = c(k)$ if the interpolation is perfect.

In the AWGN channel, the channel gain is $c(k) = 1$ and we can assume $c'(k) = c(k) = 1$ theoretically. Since the total power and the signal power do not change before and after interpolation, it can be said that the noise power in Eq. (21) is equal to that in Eq. (26). As a result, the noise power of $n_1'(k)$ becomes $\sigma_1^{'2} = \sigma^2/|z_p|^2$.

Therefore, from Eq. (27), the received symbols are given by [2]:

$$\begin{aligned} \hat{z}(k) &= \frac{z(k) + n(k)}{1 + n_1'(k)} \\ &\simeq z(k) + \{n(k) - z(k)n_1'(k)\} \end{aligned} \qquad (28)$$

and the noise power becomes $\sigma^2(1 + \sigma_z^2/|z_p|^2)$ where σ_z^2 is the power of $z(k)$.

Thus, D_2 becomes

$$D_2 = 10 \log \left(1 + \frac{\sigma_z^2}{|z_p|^2}\right) \quad \text{dB}. \qquad (29)$$

If we assume that all symbols are generated with the equivalent probability, the variance becomes $\sigma_z^2/|z_p|^2 = 5/9$; for example, if $\sigma_z^2 = 1$ then $|z_p|^2 = 9/5$, and D_2 is about 1.92 dB.

In the case of $N = 16$, D_1 is about 0.28 dB and the total degradation becomes about 2.2 dB.

Fig. 8 shows the result of the computer simulation in the AWGN channel environment. The values of $N = 16$, $N_p = 16$, and $T_s = 1/16k$ sec are adopted. The degradation is almost the same as the theoretical one calculated above, and the BER performances with three window functions are almost the same. The rectangle function in Fig. 8 means that no window function is used, which was described in [11].

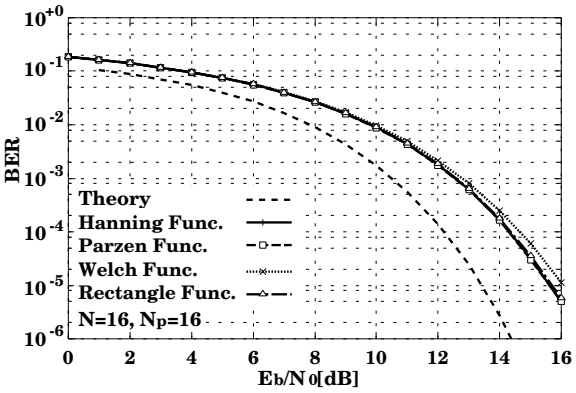

Fig. 8. BER performance of proposed scheme in AWGN channel.

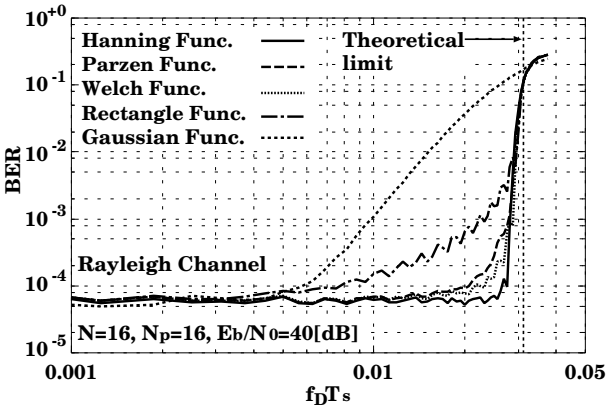

Fig. 9. Effect of the window functions.

IV. BER Performance in Rayleigh Channel

In this section we show the results of the computer simulations in Rayleigh channel with several different channel conditions.

The main restriction of the proposed method is Eq. (1), and the main parameters are N, N_p, and $f_D T_s$. By changing the values of these parameters, we can apply this scheme in various fading environments.

A. Selecting a Window Function

To compare the performance of estimation with a variety of window functions, we calculate the BER performance versus the fading pitch (Fig. 9), where $N = 16$, $N_p = 16$, and $E_b/N_0 = 40$ dB. We assume that there is no frequency offset in the received signal.

In Fig. 9, the theoretical limit of Eq. (1) is $f_D T_s = 1/32$, which is $f_D = 500$ Hz supposing $T_s = 1/16k$ sec, and the Gaussian function is the second-order Gaussian interpolation in [2]. In a relatively fast fading environment, fading estimation is greatly improved with the proposed scheme, compared with the conventional one; e.g., the Gaussian interpolation. However, the proposed scheme needs more pilot symbols. It needs to process $2NN_p$ symbols at a time for estimation and calculation. As a result, there must be

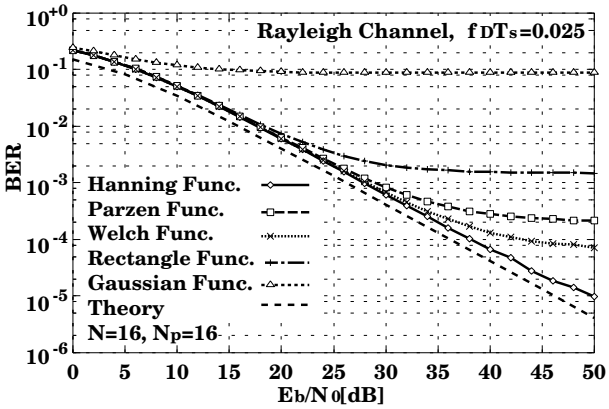

Fig. 10. BER performance in a relatively fast fading environment.

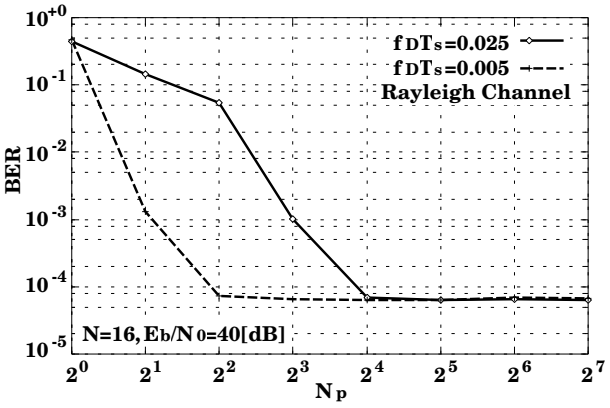

Fig. 11. BER performance versus calculating span N_p.

a large memory in this system and there will be a large calculating delay if N or N_p is large. In contrast, the second-order Gaussian scheme processes only $(2N+1)$ symbols at a time. However, with a parameter of $N = 16$, $N_p = 16$, and $T_s = 1/16k$ sec, these NN_p symbols are 256 and the cache delay is only 16 msec in the proposed scheme. The outstanding characteristic of the proposed scheme is that it can compensate very accurately until the theoretical limit is approached as shown in Fig. 9.

Next, we select the window functions. In Fig. 9, the three window functions give near BER performance. Since the one with the Hanning window function presents the best performance, we adopt the Hanning window in the following simulations.

B. BER Performance in a Relatively Fast Fading Environment

The theoretical BER of 16QAM in a Rayleigh fading environment is given in [2] by

$$P_{bray}(\gamma_0) = \int_0^\infty \frac{1}{\gamma_0} \exp\left(-\frac{\gamma}{\gamma_0}\right) P_{bnon}(\gamma) d\gamma. \qquad (30)$$

Fig. 10 shows the BER performance in a relatively fast Rayleigh fading environment where $f_D T_s = 0.025$. This condition is near the theoretical compensation limit $f_D T_s = 1/32$. The proposed scheme can compensate almost exactly, and no error floor appears even in the high E_b/N_0 region with the Hanning function.

The degradation from the theoretical curve is caused by inserting pilot symbols (D_1) and the fading estimation error (D_2). In the proposed method, this degradation occurs as follows: If the fading becomes too fast, there is a leakage of power components outside the range of $G_1(n)$ in Eq. (12), and zero symbols are inserted where they are not equal to zero actually. Then the estimate precision rapidly worsens near and above the limit of Eq. (1).

However, the degradation of the proposed scheme in Fig. 10 is about 2.2 dB from the theoretical one. This is the same as in the Gaussian channel shown in Fig. 8. Then, it can be said that $c'(k) \simeq c(k)$ even in a relatively fast Rayleigh fading environment; i.e., the proposed scheme can follow the fast fading.

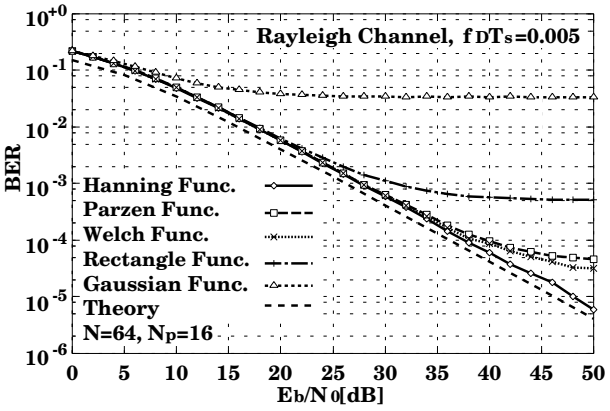

Fig. 12. BER performance in a relatively slow fading environment.

Fig. 11 shows the BER performance versus the number of received pilot symbols N_p used in fading estimation where $E_b/N_0 = 40$ dB, and $N = 16$. Since the performance with an N_p of more than $2^4 = 16$ is almost the same even in a fast fading environment $f_D T_s = 0.025$, we select $N_p = 16$ to reduce the calculation in the following.

C. BER Performance in a Relatively Slow Fading Environment

We showed that the proposed method can compensate precisely in a relatively fast Rayleigh fading environment. Next, we consider a relatively slow fading environment with a rate of $f_D T_s = 0.005$. From Eq. (1), we get $N \leq 100$. Then we let $N = 2^6 = 64$ and the results of the BER performance are shown in Fig. 12. The theoretical degradation is about 1.99 dB from Eq. (20) and (29).

The proposed method can compensate exactly, and the degradation is also near to that of the theoretical one. If we only need to consider the system in slow fading environments, we can expand the interval between the pilot symbols. The tradeoff is a large buffer memory and a calculating delay because the frame length becomes long.

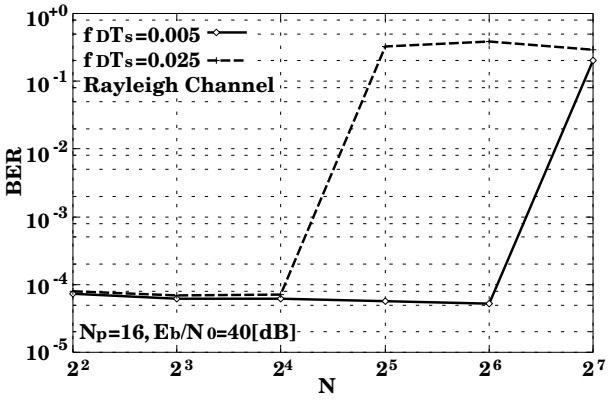

Fig. 13. BER performance versus frame length N.

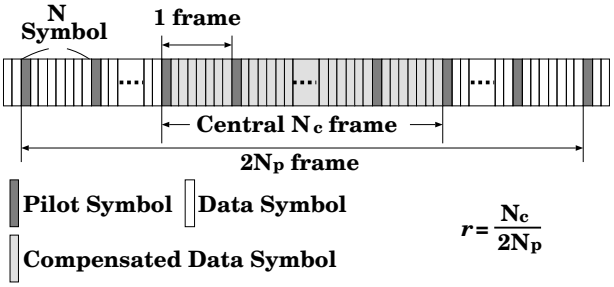

Fig. 14. Compensated frame ratio r.

Fig. 13 shows the BER performance versus the pilot symbol space N with the parameter of f_DT_s. The theoretical limit is $N \leq 20$ when $f_DT_s = 0.025$, and $N \leq 100$ when $f_DT_s = 0.005$. Beyond these limits, the BER performances degrade sharply (Fig. 13). However, it can be seen that the performance is independent of N within the limit. Thus, we can set up the pilot symbol space as large as possible.

D. Effect of the Ratio Between the Compensated Frame and the Whole $2N_p$ Frame

Up to now, a fixed ratio of $1/2$ of the compensated frames to the whole $2N_p$ calculating frames, as shown in Fig. 7, has been adopted. This ratio can be increased to improve efficiency. However, it must take values less than 1, because the value of 1 implies that the end point of a window function to be divided takes zero value. We compare the performance with various ratio r, which is defined in the following referring to Fig. 14:

$$r = \frac{N_c}{2N_p}. \tag{31}$$

Fig. 15 shows the BER performance versus the ratio r with the parameter of $E_b/N_0 = 40$ dB. The BER performance becomes worse as r closes to 1 especially when f_DT_s is 0.025. This degradation is caused by the alias effect and the effect of the AWGN. The alias effect becomes stronger and stronger as both ends of the frames are approached. When a large r is adopted, these end points are used, which results

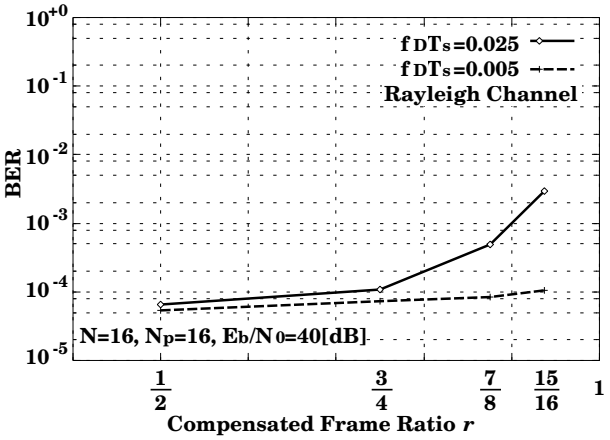

Fig. 15. BER performance versus frame ratio r.

in degradation. Moreover, since the value of the end point of the window function decreases for large r, and because this small value is used in division as a denominator in Eq. (15), the influence of AWGN also becomes relatively stronger.

Although the frame ratio of $r = 1/2$ is adopted in the continuing calculations, r may be increased to a degree of $3/4$ because the degradation against the ratio r is negligible when f_DT_S is small such as 0.005.

E. BER Performance in Fading Environments with Frequency Offset

Next we consider the carrier offset. The power spectrum of $c(t)$ including a carrier offset is given by

$$S(f) = \frac{b_0}{\pi f_D \sqrt{1 - \left(\frac{f - f_{off}}{f_D}\right)^2}} \quad (-f_D \leq f - f_{off} \leq f_D) \tag{32}$$

where b_0 is the mean received power and f_{off} is the residual frequency offset. From this equation, we know that we can compensate with the proposed scheme if the shifted spectrum is within the range of the Nyquist rate. Then, the sampling theorem including the carrier offset is given by

$$(f_D + f_{off})T_s \leq \frac{1}{2N}. \tag{33}$$

Fig. 16 shows the BER performance versus $(f_D + f_{off})T_s$ with a parameter of f_D where $E_b/N_0 = 40$ dB.

Naturally, the BER curve is similar to that of Fig. 9, and until near the limit of Eq. (33) the fading estimation is carried out almost exactly. It is also shown that the BER performance is almost flat against f_{off} in this range. The possible f_{off} range of the compensation is dependent on f_D. If f_D is small, the range becomes wide within the limit, and it becomes narrow with the large f_D. For example, at $f_DT_s = 0.005$, the tolerance of f_{off} is 340 Hz for BER= 10^{-4}, and this value decreases to 20 Hz at $f_DT_s = 0.025$. As an example, the BER performance with the parameters

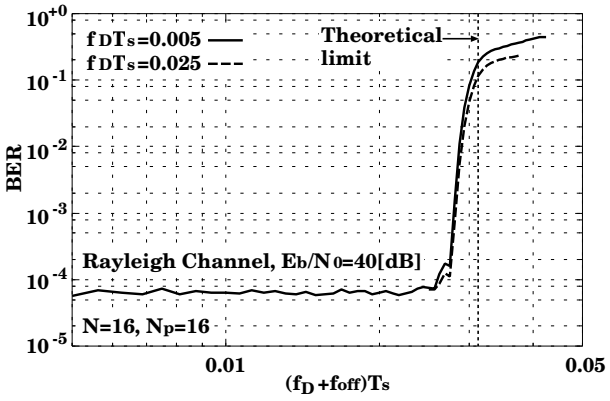

Fig. 16. BER performance versus $(f_D + f_{off})T_s$.

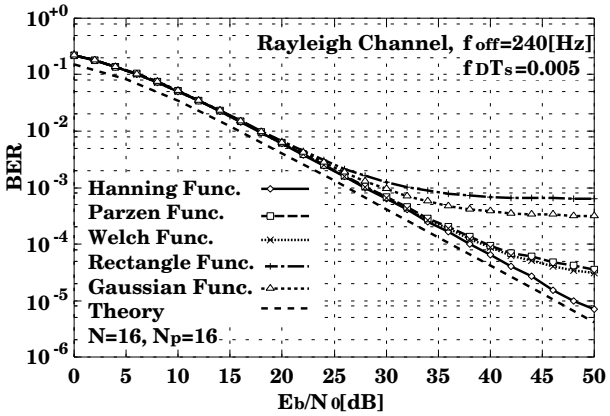

Fig. 17. BER performance in fading and frequency offset environment.

of $f_D T_s = 0.005$, and $f_{off} = 240$ Hz is shown in Fig. 17. It is shown that the proposed method can compensate the Rayleigh channel with frequency offset until the Nyquist rate is approached.

V. Conclusions

A fading compensation scheme using FFT was proposed and applied to 16QAM. This proposed scheme is a kind of PSAM. The main difference from the conventional PSAM scheme is that the proposed scheme interpolates received pilot symbols in the frequency domain instead of the time domain. The fading series becomes easier to deal with by translating received pilot symbols into the frequency domain by FFT, and the zero insertion outside of the bandwidth of the fading in the frequency domain is identical to the interpolation between the pilot symbols in the time domain. Since only zero insertion is needed, the proposed scheme is simple.

Changing the number of N_p when the interpolation is carried out is equivalent to changing the dimension of the interpolating function in the conventional method. It is difficult to consider the high order interpolating function in the time domain because of the complexity of the coefficient. However, it is possible to take a large N_p with the proposed method because the increase of N_p only changes the size of the calculation on FFT, and IFFT.

The effectiveness of this scheme was verified through computer simulations. It is shown that this scheme can compensate exactly until the Nyquist rate is approached. A certain degree of the frequency offset can also be compensated, and the possible range of the offset compensation depends on f_D.

Application of this method to other flat fading such as a Rician fading is straightforward as long as the fading is a band-limited process. Furthermore, this scheme can be applied to other modulations almost without changing, though only a 16QAM constellation has been studied in this paper.

References

[1] J. K. Cavers, "An analysis of pilot symbol assisted modulation for Rayleigh fading channels," *IEEE Trans. Veh. Technol.*, vol. 40, pp. 686-693, Nov. 1991.

[2] S. Sampei and T. Sunaga, "Rayleigh fading compensation for QAM in land mobile radio communications," *Trans. IEEE Trans. Veh. Technol.*, vol. 42, pp. 137-147, May. 1993.

[3] H.-B. Li, Y. Iwanami, and T. Ikeda, "Symbol error rate analysis for MPSK under Rician fading channels with fading compensation based on time correlation," *IEEE Trans. Veh. Technol.*, vol. 44, pp. 535-542, Aug. 1995.

[4] D. Subasinghe-Dias and K. Feher, "A coded 16 QAM scheme for fast fading mobile radio channels," *IEEE Trans. Com.*, vol. 43, pp. 1906-1916, May 1995.

[5] T. Sunaga and S. Sampei, "Performance of multi-level QAM with post-detection maximal ratio combining space diversity for digital land-mobile radio communications," *IEEE Trans. Veh. Technol.*, vol. 42, pp. 294-301, Aug. 1993.

[6] J. K. Cavers, "Pilot symbol assisted modulation and detection in fading and delay spread," *IEEE Trans. Com.*, vol. 43, pp. 2206-2212, Jul. 1995.

[7] E. O. Brigham, *The fast fourier transform*, Prentice-Hall, 1974.

[8] W. C. Y. Lee, "Estimate of channel capacity in Rayleigh fading environment," *IEEE Trans. Veh. Technol.*, vol. 39, pp. 187-189, Aug. 1990.

[9] P. M. Fortune, L. Hanzo and R. Steele, "On the computation of 16-QAM and 64-QAM performance in Rayleigh-fading channel," *IEICE Trans.*, vol. E75-B, pp. 466-475, Jun. 1992.

[10] R. E. Ziemer and R. L. Peterson, *Digital Communications and Spread Spectrum Systems.* New York: Macademian, 1985, pp. 207-212.

[11] E. Okamoto, H.-B. Li and T. Ikegami, "Rayleigh fading compensation for QAM by using FFT," in *Proc. IEEE PIMRC'96*, Taipei, ROC, Oct. 1996, pp. 1079-1082.

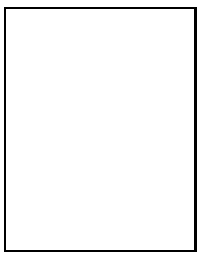

Eiji Okamoto was born in Chiba, Japan, in 1970. He received the B.E. and M.S. degrees in Electrical Engineering from Kyoto University, Japan, in 1993 and 1995 respectively. Since 1995, he has been with the Communications Research Laboratory (CRL), at the Ministry of Posts and Telecommunications, Japan, where he has been researching coded modulation and fading compensation for land and satellite mobile communication systems. Mr. Okamoto is a member of the Institute of Electronics, Information and Communication Engineers (IEICE), Japan.

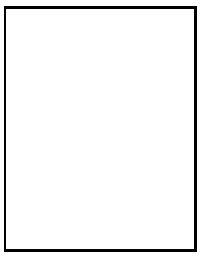

Huan-Bang Li was born in Ji Lin province, P. R. China, on July 11, 1964. He received the B.S. degree in Telecommunications and Control Engineering from Northern Jiao Tong University, Beijing, China in 1986. He received the M.S. and the Dr. of Eng. degrees in Electrical and Computer Engineering from Nagoya Institute of Technology, Nagoya, Japan in 1991 and 1994 respectively. He joined the Communications Research Laboratory (CRL), at the Ministry of Posts and Telecommunications, Japan in 1994. He is now a senior researcher of the Kashima Space Research Center of CRL. His major research interest is on digital communications, mobile communications and bandwidth-efficient modulations. He is currently engaged in research on coded modulation and experimental research on satellite communications. He received the Young Engineer Award of IEICE Japan in 1996.

Dr. Li is a member of the IEICE of Japan.

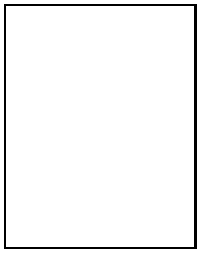

Tetsushi Ikegami was born in Tokyo, Japan, in 1957. He received the B.E., M.E. and Dr. E. degrees all in electrical engineering from Meiji University, Kawasaki, Japan in 1980, 1982, 1995 respectively. In 1985 he joined the Communications Research Laboratory, at the Ministry of Posts and Telecommunications, and has been engaged in the development of mobile, fixed and inter satellite communication systems. From 1991 to 1992 he was a visiting scholar at the University of Illinois at Urbana-Champaign. Since 1997, he has been with the Department of Electronics and Communications, School of Science and Technology, Meiji University, where he is currently an Associate Professor. His research interests are in the areas of satellite and fading channels, modulation, coding and spread spectrum systems.

Dr. Ikegami is a member of SITA and IEEE.